

# On-Particle Rolling Circle Amplification-Based Core-Satellite Magnetic Superstructures for MicroRNA Detection

**Tian, Bo; Qiu, Zhen; Ma, Jing; Donolato, Marco; Hansen, Mikkel Fougt; Svedlindh, Peter; Strömberg, Mattias**

*Published in:*
A C S Applied Materials and Interfaces

*Link to article, DOI:*
10.1021/acsami.7b16293

*Publication date:*
2018

*Document Version*
Peer reviewed version

Article

# On-Particle Rolling Circle Amplification Based Core-Satellite Magnetic Superstructures for MicroRNA Detection

Bo Tian, Zhen Qiu, Jing Ma, Marco Donolato, Mikkel Fougt Hansen, Peter Svedlindh, and Mattias Strömberg

*ACS Appl. Mater. Interfaces*, **Just Accepted Manuscript** • DOI: 10.1021/acsami.7b16293 • Publication Date (Web): 21 Dec 2017

# On-Particle Rolling Circle Amplification Based Core-Satellite Magnetic Superstructures for MicroRNA Detection

Bo Tian,[†] Zhen Qiu,[†] Jing Ma,[‡] Marco Donolato,[§] Mikkel Fougt Hansen,[#] Peter Svedlindh,[†] and Mattias Strömberg*,[†]

[†] Department of Engineering Sciences, Uppsala University, The Ångström Laboratory, Box 534, SE-751 21 Uppsala, Sweden

[‡] Department of Immunology, Genetics and Pathology, Uppsala University, The Rudbeck Laboratory, SE-751 85 Uppsala, Sweden

[§] BluSense Diagnostics, Fruebjergvej 3, DK-2100 Copenhagen, Denmark

[#] Department of Micro- and Nanotechnology, Technical University of Denmark, DTU Nanotech, Building 345B, DK-2800 Kongens Lyngby, Denmark

**ABSTRACT:** Benefiting from the specially tailored properties of the building blocks as well as of the scaffolds, DNA-assembled core-satellite superstructures have gained increasing interest in drug delivery, imaging and biosensing. The load of satellites plays a vital role in core-satellite superstructures and it determines the signal intensity in response to a biological/physical stimulation/actuation. Herein, for the first time, we utilize on-particle rolling circle amplification (RCA) to prepare rapidly responsive core-satellite magnetic superstructures with a high load of magnetic nanoparticle (MNP) satellites. Combined with duplex-specific nuclease assisted target recycling, the proposed magnetic superstructures hold great promise in sensitive and rapid microRNA detection. The long single-stranded DNA produced by RCA serving as the scaffold

of the core-satellite superstructure, can be hydrolyzed by duplex-specific nuclease in the presence of target microRNA, resulting in a release of MNPs that can be quantified in an optomagnetic sensor. The proposed biosensor has a simple mix-separate-measure strategy. For let-7b detection, the proposed biosensor offers a wide linear detection range of approximately five orders of magnitude with a detection sensitivity of 1 fM. Moreover, it has the capability to discriminate single-nucleotide mismatches and to detect let-7b in cell extracts and serum, thus showing considerable potential for clinical applications.

**KEYWORDS:** *on-particle rolling circle amplification, core-satellite superstructures, magnetic nanoparticles, microRNA detection, optomagnetic biosensor*

## INTRODUCTION

Point-of-care diagnostics is one of the principal motivations behind the current development of nanotechnology. The various requirements for point-of-care diagnostics, *e.g.*, ease-of-use, short assay time, high sensitivity and low cost, are challenging for traditional analytical methods and in most cases beyond the capability of monofunctional-material-based biosensors.[1-3] In order to strengthen the performance of biosensors, materials with different functionalities are commonly used simultaneously. In contrast to the utilization of a mixture of different materials, using the assembly of various simple building blocks offers further improvement of the biosensing performance, and has a much broader range of applications since it takes advantage of both the intrinsic and collective properties of the constituents.[4-7] Owing to the predictability, specificity, and diversity of hybridization, DNA as a scaffold/spacer shows great potential in assembling nano- to micron-sized superstructures.[8-11] In particular, the use of DNA-assembled core-satellite superstructures in biosensing applications enables control of the dimension, composition, functionality of the core/satellite building blocks and of the sequence of DNA scaffold/spacer. It is thereby a flexible tool to meet the requirements for clinical diagnostics.[12-18]

In our previous work, a multilayer core-satellite magnetic superstructure was reported for RNA biosensing.[19] As a consequence of the duplex-specific nuclease (DSN) assisted DNA hydrolysis, satellites were released from the core-satellite magnetic superstructures into the suspension and measured. The as-reported multilayer core-satellite magnetic superstructure offered advantages of: (a) easy manipulation because of the magnetic micron-sized core, (b) multiplexing because of the controllable release of different nano-sized satellites, and (c) predictable enzyme-based reactions because of the programmable DNA scaffold/spacer. However, the layer-by-layer material preparation, *i.e.*, conjugating one end of the DNA probes to the surface of the core

followed by conjugating satellites to the other end of the DNA probes, limited the load of satellites and thus affected the sensitivity of the biosensor. Additionally, in this preparation method, satellites were often linked to the core *via* more than one DNA probe, which further reduced the sensitivity of the biosensor since several DNA hydrolysis reactions were required to release a single satellite.[13,19]

In order to address the issues faced by layer-by-layer preparation based core-satellite superstructures, we herein take advantage of an on-particle rolling circle amplification (RCA) based method for improved preparation of core-satellite magnetic superstructures. RCA is a simple and efficient isothermal amplification tool that produces long single-stranded DNA (ssDNA) molecules with programmable repeating sequences, which can further be utilized as scaffolds for assembling nanostructures into one-dimensional superstructures.[20-23] Moreover, the RCA reaction can be performed on the surface of a particle (on-particle RCA) followed by assembling nano-sized satellites, which provides programmable three-dimensional core-satellite superstructures.[24-28] Here, we develop on-particle RCA with biotinylated DNA building blocks to prepare core-satellite magnetic superstructures with a high load of magnetic nanoparticle (MNP) satellites. The on-particle RCA products contain repeating sequences that can hybridize to target RNAs, forming DNA:RNA heteroduplex structures, which can subsequently be cleaved by DSN. The RNA strands are preserved in the hydrolysis and then released to the suspension to trigger more reactions. This process, denoted DSN-assisted target recycling,[29-34] cleaves on-particle RCA based core-satellite superstructures and releases one-dimensional assemblies of MNPs. The one-dimensional superstructures can be further cleaved as the DSN-assisted target recycling continues to release individual MNPs.

MicroRNAs are 19 to 23-nucleotide long tissue-specific biomarkers for tumor progression and metastasis.[35-38] Standard RNA analysis strategies, *i.e.*, Northern blotting,[39,40] oligonucleotide microarrays,[41,42] and quantitative reverse transcription polymerase chain reaction (qRT-PCR),[43,44] have been widely used for microRNA analysis, but still have their own limitations, *e.g.*, low sensitivity, labor-intensive processes, or lack of 5´-end specificity.[45,46] By the combination of on-particle RCA based core-satellite magnetic superstructures, DSN-assisted target recycling and the 405 nm laser-based optomagnetic sensor, we demonstrate a homogeneous and volumetric detection biosensor for microRNA. Relying on the high load of MNPs, the on-particle RCA based method shows improvements in terms of response speed, signal amplitude and sensitivity in comparison with our previous work which used layer-by-layer assembled core-satellite magnetic superstructures. As far as we know, this is the first demonstration of a biosensor based on the combination of RCA and DSN-assisted target recycling.

## RESULTS AND DISCUSSION

**Detection Principle.** On-particle RCA produces long ssDNA containing repeating DNA sequences that are complementary to the target RNA, *i.e.*, let-7b used in this study. The ssDNA is serving as a scaffold to assemble MNPs onto micro-particle (MP) cores to form on-particle RCA based core-satellite superstructures (MP-RCA-NPs). Target RNA molecules present in the suspension can hybridize to the ssDNA scaffolds to form DNA:RNA heteroduplexes, which can be recognized and cleaved by DSN, resulting in a release of MNPs from the MP-RCA-NP superstructures. The target RNA is preserved in the DSN-based hydrolysis and is thus able to

bind to other complementary sequences on the same or on another ssDNA scaffold. The working principle is schematically illustrated in **Figure 1**.

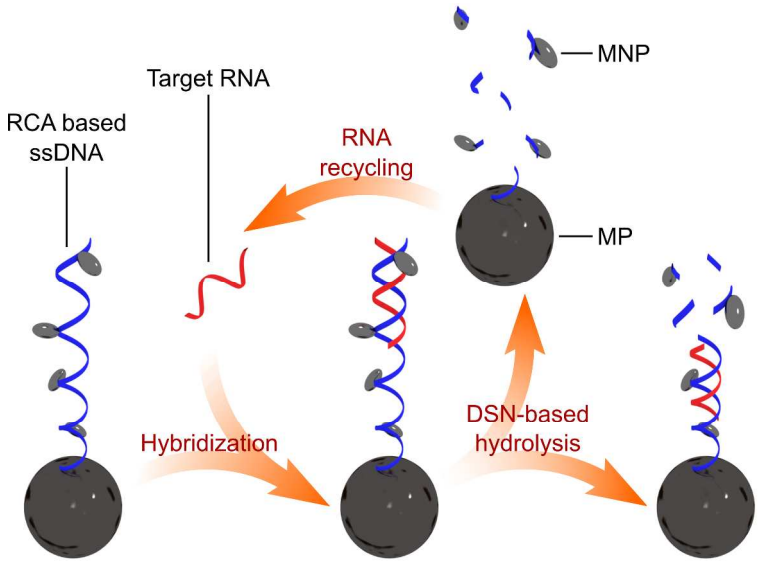


**Figure 1.** Working principle of microRNA detection based on MP-RCA-NP superstructures and DSN-assisted target recycling. Target RNA hybridizes to an ssDNA scaffold and forms a DNA:RNA heteroduplex. The DNA:RNA heteroduplex is cleaved by DSN and MNPs are subsequently released. The target RNA is preserved in the reaction and is thus able to bind to other complementary sequences on the same or on another ssDNA scaffold.

MNPs released to the suspension are quantified with a 405 nm laser-based optomagnetic sensor. The sensor records the second harmonic modulation of the transmitted light intensity in response to an applied field $B(t)=B_0\sin(2\pi ft)$. The output signal, $V_2'/V_0$, is the real ($\sin(4\pi ft)$) part of the second harmonic component of the transmitted light intensity normalized by the simultaneously measured total transmitted light intensity. A typical $V_2'/V_0$ spectrum in this study is characterized by a peak located around 200 Hz representing the response from suspended MNPs,

which is used for the quantification of target microRNA. Detailed description as well as the underlying theory of the 405 nm laser-based optomagnetic sensor can be found in our previous publications.[47-51]

**Characterization of On-Particle RCA Based Core-Satellite Magnetic Superstructures.** To prepare MP-RCA-NP superstructures, biotinylated dUTPs are used to replace a part of dTTPs as DNA building blocks during the on-particle RCA. The utilization of biotin-dUTP results in ssDNA products containing biotin groups that can subsequently assemble streptavidin coated MNPs. To study the performance of the MP-RCA-NP superstructures and to compare with ssDNA probe based MP-NP superstructures, on-particle RCA reactions were performed with high or low biotin-dUTP concentrations, by employing biotin-dUTP:dTTP ratios of 3:1 or 1:3, respectively. In **Figure 2a** and **b** scanning electron microscopy (SEM) micrographs are shown for MP-RCA-NP superstructures with high or low MNP loads, respectively. From the SEM micrographs it can be concluded that the MNPs are assembled on the MP cores. Due to the assembly of several MNPs on the same ssDNA molecule forming a random-coil structure, drying effect, and the nonspecific binding between nearby ssDNA strands, MNPs are not uniformly distributed but form islands on the MP-RCA-NP superstructures. The size of MNP islands is influenced by the concentration of biotin-dUTP used in RCA, *i.e.*, a higher biotin-dUTP:dTTP ratio leads to a higher MNP load of the superstructure and thus larger MNP islands on MPs. As a comparison, **Figure 2c** shows the morphology and structure of the ssDNA probe based MP-NP superstructures, on which the MNPs are uniformly distributed.

The sensitivity and accuracy of core-satellite superstructure based biosensors are strongly influenced by the load of releasable MNP satellites. To evaluate the capability of releasing MNPs, three different kinds of core-satellite superstructures (MP-RCA-NPs with high MNP load, MP-RCA-NPs with low MNP load and MP-NPs) were reacted with 10 nM of let-7b to cleave ssDNA through DSN-assisted target recycling. For the MP-RCA-NPs with high and low MNP loads, the signal increased at a higher rate than for the MP-NPs during the first 30 min of the reaction. This implies that fewer DSN-based hydrolysis reactions were needed for MP-RCA-NPs to release MNPs (cf. slopes of lines in **Figure 2d**). Due to the layer-by-layer preparation of the MP-NP superstructures, MNPs were linked to the MP core *via* more than one ssDNA probe, resulting in a slower response to targets.[19] From analysis of the concentration of MNPs released from the superstructures after an incubation time of 90 min, the average ratios between MP cores and MNP satellites were calculated to 1:143, 1:75 and 1:73 for MP-RCA-NPs with high MNP load, MP-RCA-NPs with low MNP load and MP-NPs, respectively (Supporting Information, **section S1**). Although the MP-RCA-NPs with low MNP load and MP-NPs have similar MP:MNP ratio, their arrangement and distribution of MNP satellites are very different.

The arrangement of MNPs on the RCA products is another critical parameter that influences the analytical performance of the MP-RCA-NP superstructures. Biotin groups are randomly distributed along the ssDNA. A high MNP load means a high-density arrangement of MNPs on the ssDNA (illustration in **Figure 2a**). Moreover, since there are more target-recognizing sequences between two nearby MNPs on the same ssDNA for a low-density MNP arrangement (illustration in **Figure 2b**), fewer MNPs are released by each DSN-based hydrolysis reaction, resulting in a lower rate of the signal increase, see **Figure 2d** where blue circles and red

diamonds represent high-density and low-density MNP arrangements, respectively. However, since the target recognizing sequences in the ssDNA also contain biotin groups that can bind to the MNPs, a high-density MNP arrangement may hinder the hybridization of target microRNA as well as the DSN-based hydrolysis, which leads to an increased number of un-releasable MNPs. Despite this small drawback, we still chose MP-RCA-NP with a high-density MNP arrangement for the following experiments to obtain a better accuracy with a quicker response.

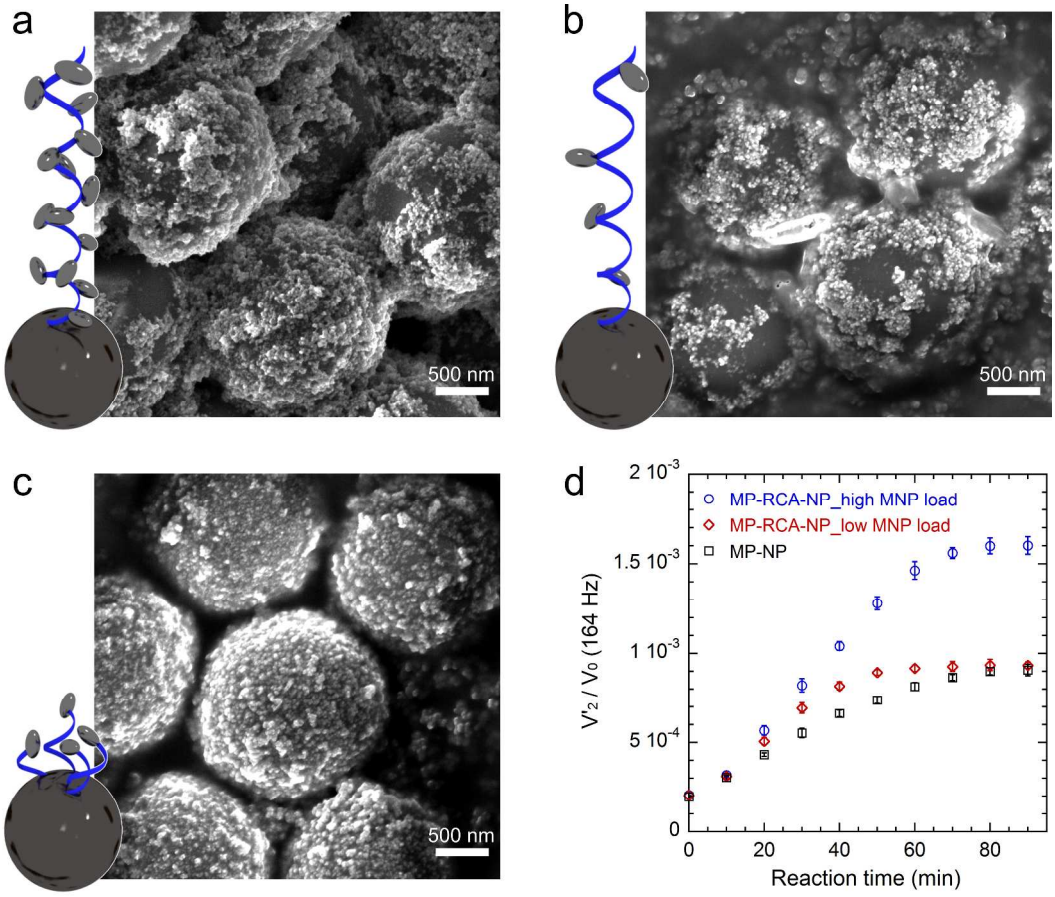


**Figure 2.** Representative SEM micrographs of (a) MP-RCA-NP superstructures with a high MNP load, (b) MP-RCA-NP superstructures with a low MNP load, and (c) ssDNA probe based MP-NP superstructures. (d) Time-resolved peak amplitude increase for three different core-

satellite superstructures reacted with 10 nM of let-7b. All the measurements were performed three times independently and the standard deviations were plotted as error bars.

**Quantitative MicroRNA Detection.** The quantification of target microRNA using the high MNP load MP-RCA-NPs was investigated. The target RNA, let-7b, was diluted by the reaction buffer to a series of concentrations ranging from 1 μM to 10 aM, followed by reaction with MP-RCA-NPs and DSN cleaving for 60 min. Thereafter, the concentration of MNPs in the suspension, mainly released from the core-satellite superstructures (see Supporting Information, **section S1**), was measured by the optomagnetic sensor. As shown in **Figure 3a**, the peak in the $V_2'/V_0$ spectra, representing the signal from suspended 100 nm MNPs, increased monotonously with increasing let-7b concentration. Although centrifugation was adopted as the last step in the preparation protocol for the superstructures to remove unbound MNPs, it could not provide conditions for complete removals, thereby resulting in a background signal for all of the measurements. When measuring low target concentrations, the peak positions were slightly shifted to the low-frequency region, implying the presence of suspended dimers and/or short chains of MNPs. **Figure 3b** shows the $V_2'/V_0$ peak amplitudes plotted against the target concentration. From the dose-response curve it can be seen that the linear detection range spans over approximately five orders of magnitude (10 fM to 1 nM) and that there exists a signal plateau at high target concentrations (≥ 10 nM). The red dashed line in **Figure 3b** indicates the cutoff value, which was calculated based on the three-sigma criterion, *i.e.*, the average peak value of the blank controls plus three times of their standard deviations. The limit of detection (LOD) of the proposed biosensor, defined as the lowest target concentration that can generate a peak amplitude higher than the cutoff value, was obtained as 1 fM. The average coefficient of

variation (CV) was 4.1%, indicating high reproducibility. The major factors which cause variations in measured peak amplitudes are most likely sample-to-sample variations in the concentration of superstructures and temperature fluctuations during the DSN-assisted release of MNP satellites. For plasma, the total microRNA concentration was reported to be at the 100 fM level,[52] implying that the femtomolar level LOD provided by the proposed biosensor is sufficient for microRNA analysis in plasma. It should be emphasized that the LOD and detection range can be further adjusted by simply choosing different reaction times for DSN-assisted target recycling.

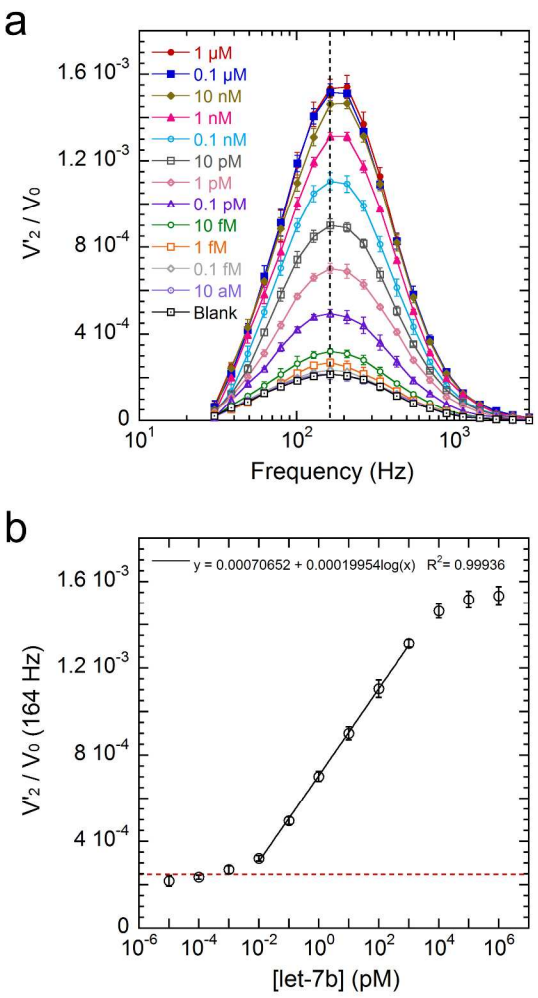

**Figure 3.** Optomagnetic spectra (a) and dose-response curve (b) for MP-RCA-NP superstructure (high MNP load) based quantification of let-7b. The black dashed vertical line in (a) indicates the peak position at 164 Hz. The black solid line and the red dashed line in (b) indicate the linear detection range and the cutoff value, respectively. All the measurements were performed three times independently and the standard deviations were plotted as error bars.

Compared to the MP-NP superstructure based microRNA detection in our previous work,[19] the MP-RCA-NP based biosensing shows improvements in both signal amplitude and reaction speed. Relying on the high load of MNP satellites, MP-RCA-NP superstructures can release more MNPs than MP-NP superstructures, thereby offering almost doubled optomagnetic peak amplitudes without increasing CVs and thus improved accuracy. In addition, since fewer DSN-based hydrolysis reactions are needed for MP-RCA-NPs than for MP-NPs to release a certain number of MNPs, MP-RCA-NPs show a faster response to target molecules present in low concentrations. However, MP-RCA-NPs release chains of MNPs instead of individual ones when reacted with target molecules of low concentrations; these chains have very low optomagnetic signals and nearly negligible contributions to the peak amplitude located around 200 Hz, which influences the sensitivity of the proposed biosensor. As a result, the MP-RCA-NP based biosensor is approximately 5 times more sensitive than the previous method based on MP-NP superstructures.

The widespread use of the DSN-assisted target recycling strategy allows for a convenient comparison between the proposed biosensor and previously published DSN-based biosensors. For reported biosensors using 0.5-1.5 h of DSN-assisted target recycling, LODs of 60 aM

(electrochemical impedance spectroscopy),[53] 0.1 fM (UV-vis spectroscopy),[54] 0.3 fM (surface-enhanced Raman spectroscopy),[55] 0.5 fM (UV-vis spectroscopy),[56] 3.36 fM (magnetic relaxation switch sensor),[31] 1 pM (UV-vis spectroscopy),[34] 1.03 pM (fluorescence spectroscopy)[33] and 1.1 pM (fluorescence spectroscopy)[57] were reported for the detection of different microRNAs. However, except for the magnetic relaxation switch biosensor, all these biosensors need additional pretreatment, washing or signal generation steps, which limit their potential for point-of-care applications. In comparison, the proposed MP-RCA-NP superstructure based optomagnetic biosensor has a simple mix-separate-measure strategy which can be easily integrated into microfluidic systems.[58]

**Specificity Test.** Due to the strong sequence homology between different microRNAs within the same family discrimination between these is complicated. The specificity of the proposed method for let-7b against other control microRNAs was tested by comparing the optomagnetic peak amplitudes obtained from 0.1 nM of different let-7 microRNAs (using MP-RCA-NPs with a high MNP load, **Figure 4**). Sequences of the let-7 microRNAs measured in this study and the differences among them are summarized in **Table S2**. The two highest nonspecific signals, obtained from 0.1 nM of let-7c (single-nucleotide mismatches) and 0.1 nM of let-7a (double-nucleotide mismatches), were found to be equal to the signals of 1.7 and 0.3 pM of let-7b, respectively. Nonspecific signals were induced by the 16-bp-long perfect DNA:RNA heteroduplexes formed between the non-target microRNAs (let-7c and let-7a) and the recognition sequences on the RCA products. From the results of the specificity test it is evident that the proposed method is capable of discriminating between sequences containing even single-nucleotide mismatches.

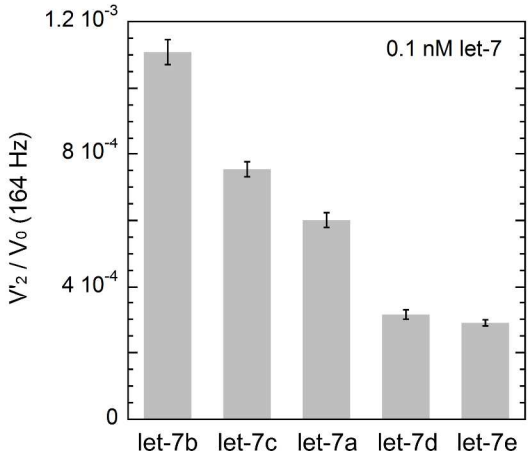


**Figure 4.** Specificity test for the proposed let-7b detection method using high MNP load MP-RCA-NPs. Optomagnetic peak amplitudes for five different types of let-7 microRNA (0.1 nM) are shown. All the measurements were performed three times independently and the standard deviations were plotted as error bars.

**Detection of Endogenous MicroRNA from HeLa Cells.** Total RNAs that were extracted from human cervical cancer cells (HeLa) were investigated to demonstrate the performance of the MP-RCA-NP superstructure for target quantification in cell extracts. Cell extracts (containing total RNAs) were diluted by the reaction buffer to an RNA concentration of 1 μg $mL^{-1}$ to serve as the pure extracts. Spiked samples containing 1, 10, 100 and 1000 pM of synthetic let-7b were prepared by spiking the target RNA into pure extracts. The optomagnetic spectra and signals of the pure and spiked RNA extracts are shown in **Figure 5**. For the spectra of RNA extracts (**Figure 5a**), no shape change was observed (compare with **Figure 3a**). The let-7b concentration of the pure extracts was found to be 39.7 ± 3.3 fM (corresponding to 2.387 ± 0.196 × $10^7$ copies $\mu g^{-1}$ total RNA) by calculating the linear fitting of the peak amplitudes obtained from the four spiked RNA extracts, which agrees well with the result obtained by qRT-PCR (44.3 ± 3.7 fM).

The results suggest that the MP-RCA-NP based biosensor is suitable for clinical diagnosis and prognosis applications.

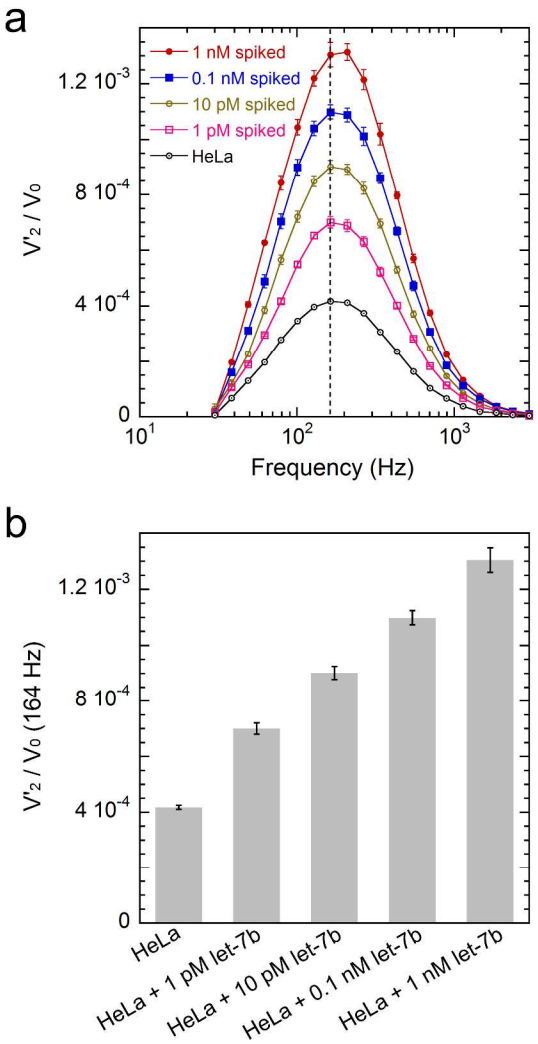


**Figure 5.** Optomagnetic spectra (a) and peak amplitude (b) obtained from diluted total RNA extracts (containing 1 μg $mL^{-1}$ total RNA) spiked with let-7b. The black dashed vertical line in (a) indicates the peak position at 164 Hz. All the measurements were performed three times independently and the standard deviations were plotted as error bars.

**Matrix Effects and Serum Detection.** Apart from tissues, microRNAs are also circulating in body fluids such as plasma.[52,59] Since cell extracts have limited matrix effects, the robustness of the biosensor was further studied by using fetal bovine serum (FBS, diluted with reaction buffer, **Figure 6**). Except for increasing the viscosity of the suspension, the matrix effects of FBS mainly include: (1) inducing MNP aggregation, and (2) inhibiting the DSN-based reaction. To evaluate the aggregation effect, MNPs (35 μg $mL^{-1}$) in different FBS solutions were measured. No significant MNP aggregation was found at FBS concentrations lower than 40% (cf. **Figure 6a** and **S2a**). However, when the MP-RCA-NP (high MNP load) based biosensor was utilized to detect 0.1 μM of let-7b in FBS solutions (**Figure 6a** and **S2b**), the optomagnetic signals were much lower compared to the direct suspension of MNPs, implying the inhibition caused by FBS (RNA binding proteins, nonspecific oligonucleotides, RNase, *etc.*).

We further performed let-7b quantification in FBS using the MP-RCA-NP superstructures (high MNP load). The target RNA was spiked into 20% FBS to a series of concentrations and measured. Compared to the measurements performed in buffer solutions (**Figure 3b**), the dose-response curve shown in **Figure 6b** has a narrower linear detection range from 0.1 pM to 1 nM. Moreover, matrix effects influenced the biosensing performance and resulted in a weakened LOD of 10 fM. Considering that the real serum samples in clinical diagnostics are much more complex than FBS, RNA extraction is recommended before microRNA analysis. Spectra of the optomagnetic measurements are shown in **Figure S2c**.

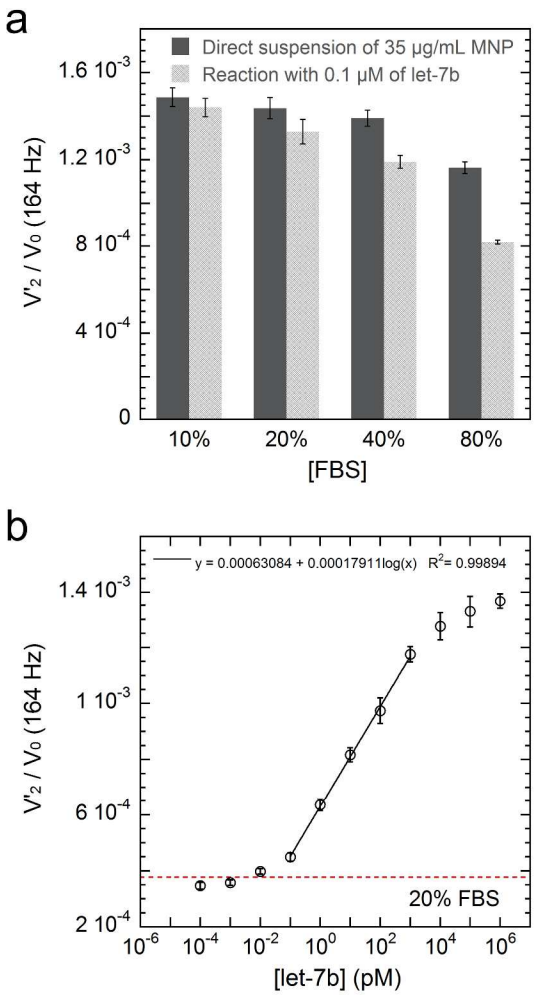


**Figure 6.** Stability study in FBS. (a) Bar graph of the optomagnetic signal at 164 Hz for direct MNP measurement and for MP-RCA-NP based let-7b detection in diluted FBS samples. (b) dose-response curve for MP-RCA-NP (high MNP load) based quantification of let-7b. The black solid line and the red dashed line in (b) indicate the linear detection range and the cutoff value, respectively. All the measurements were performed three times independently and the standard deviations were plotted as error bars.

## CONCLUSIONS

In this study, on-particle RCA based core-satellite magnetic superstructures were prepared and combined with DSN-assisted target recycling for optomagnetic detection of microRNA. As far as we know, this is the first demonstration of a biosensor based on the combination of RCA and DSN-assisted target recycling. Compared to the MP-NP superstructures reported by us in earlier work,[19] the as-prepared MP-RCA-NPs have a doubled load of MNP satellites and need fewer hydrolysis reactions to release MNPs, thus providing improved sensing accuracy as well as sensitivity. The proposed biosensor offers a wide linear detection range (10 fM to 1 nM) with a detection sensitivity of 1 fM for let-7b detection. We have also demonstrated the ability of the proposed method to discriminate single-nucleotide mismatches and to detect let-7b in cell extracts and serum. Despite the advantages mentioned above, the MP-RCA-NP superstructure based method has some limitations for biosensing applications: (1) micro-particles easily aggregate and precipitate during the on-particle RCA process, thereby limiting the length of the RCA products; (2) a separation step is needed to remove the micro-particles after the DSN-based reaction since the micro-particles influence the optomagnetic measurement. To further improve the detection strategy to achieve a mix-measure format, MNP chains could be considered in a follow-up study. In this study RCA products serve as scaffolds to stabilize MNP chains formed in a rotating magnetic field,[60] thereby preparing one-dimensional superstructures that can be used for microRNA detection. In summary, by utilizing the special properties of MP-RCA-NP superstructures, DSN-assisted target recycling and optomagnetic sensing, we have presented a sensitive, rapid, homogeneous and isothermal microRNA detection method in a simple mix-separate-measure format that can be added to the toolbox for versatile clinical applications, *e.g.*,

magnetic actuation based tissue engineering, magnetic field controlled drug delivery and hyperthermia therapy.

## MATERIALS ANDMETHODS

**DNA and RNA Sequences.** DNA sequences including biotinylated template and padlock probe were used for on-particle RCA. Single-stranded DNA probes were used for assembling MP-NP superstructures. RNA sequences including let-7b, let-7c, let-7d and let-7e were used as the target or controls. DNA and RNA sequences are listed in **Table S2**. All sequences were synthesized by Biomers (Ulm, Germany) and dissolved in 50 mM Tris-HCl (pH 8.0) for storage at -20°C.

**Chemicals.** RNase inhibitor (20 U $\mu L^{-1}$), Tris-HCl (1 M, pH 8.0), φ29 polymerase, φ29 buffer, ATP, T4 ligase, dA/T/C/GTP, biotin-11-dUTP and bovine serum albumin were purchased from Thermo Fisher Scientific (Waltham, USA). Duplex-specific nuclease was purchased from Evrogen (Moscow, Russia), dissolved in Tris-HCl (50 mM, pH 8.0) and glycerol (at 1:1 ratio) for storage at -20°C. DTT, glycerol, biotin, $MgCl_2$ and FBS were purchased from Sigma-Aldrich (St. Louis, USA). Phosphate buffered saline (PBS, 20×) was purchased from AMRESCO (Solon, USA). For DSN-based reaction, the reaction buffer consisted of Tris-HCl (50 mM, pH 8.0), 20 mM $MgCl_2$ and 1 mM DTT. Streptavidin coated 100 nm MNPs (multicore magnetic beads containing clusters of small single domain particles, $6\times10^{12}$ particles $mL^{-1}$, 10 mg $mL^{-1}$, product code 10-19-102) and streptavidin coated magnetic microparticles ($5.5\times10^{9}$ particles $mL^{-1}$, 25 mg $mL^{-1}$, product code 08-19-203) were purchased from Micromod Partikeltechnologie GmbH (Rostock, Germany). All the pipette tips and storage tubes were RNase-free.

**Preparation of RCA Template Conjugated Magnetic Microparticles.** Streptavidin coated MPs (2.5 mg, 100 μL of the stock solution) were washed twice and resuspended in 200 μL PBS (1×) before conjugation. Biotinylated RCA template (10 μL, 1 μM) was pipetted into the MP suspension for conjugation (20°C, 20 min). Thereafter biotin (100 μL, 1 mM) was added to the suspension for blocking, and the suspension was incubated at 20°C for 10 min. The blocked template-MPs were washed three times by a magnetic stand to remove unused template and biotin, and finally resuspended in 400 μL $H_2O$.

**Synthesis of MP-RCA-NP Core-Satellite Magnetic Superstructures by On-Particle RCA.** The ligation mixture (500 μL) for on-particle RCA was prepared by mixing 50 μL of 10×φ29 buffer, 25 μL of ATP (20 mM), 10 μL of padlock probe (1 μM), 10 μL of T4 ligase (1 U $\mu L^{-1}$), 400 μL of as-prepared template-MPs and 10 μL of $H_2O$, followed by incubation at 37°C for 15 min. For on-particle RCA reaction (to prepare MP-RCA-NP superstructures with high MNP load), 500 μL of ligation mixture (containing 2.5 mg of MPs) was mixed with 30 μL of 10×φ29 buffer, 75 μL of dNTPs (containing 0.25 mM of dTTP, 1 mM each of dATP, dCTP and dGTP), 75 μL of biotin-11-dUTP (0.75 mM), 75 μL of BSA (2 μg $\mu L^{-1}$) and 25 μL of φ29 polymerase (10 U $\mu L^{-1}$), followed by incubation at 30°C for 60 min with gentle shaking. Aggregates of MPs formed during the RCA reaction by coiling and nonspecific binding of ssDNA. The aggregates can be unfolded by incubating the suspension at 65°C for 10 min. Thereafter the on-particle RCA products were washed three times with 50 mM Tris-HCl (65°C) using a magnetic separation stand, followed by adding 100 μL of streptavidin coated 100 nm MNPs (10 mg $mL^{-1}$) and incubating at 60°C for 15 min to form MP-RCA-NP superstructures. Unbound MNPs were removed by five times of centrifugation using a VWR Galaxy MiniStar microcentrifuge (2000 g,

10 s). Lastly, the MP-RCA-NP superstructures were resuspended in Tris-HCl (200 μL, 50 mM) for storage at 4°C. For the preparation of MP-RCA-NP superstructures with low MNP load, the synthesis procedure was similar except for reducing the ratio of biotin-dUTP:dTTP from 3:1 to 1:3.

**Synthesis of MP-NP Core-Satellite Magnetic Superstructures by ssDNA Probes.** Streptavidin coated MPs (2.5 mg, 100 μL of the stock solution) were washed twice and resuspended in Tris-HCl (50 mM, pH 8.0). Biotinylated ssDNA probes (120 μL, 100 μM) were added into the MP suspension for conjugation (20°C, 20 min). After that, the ssDNA probe-MPs were washed three times by a magnetic stand to remove unused probes, and resuspended in Tris-HCl (100 μL, 50 mM). Streptavidin coated 100 nm MNPs (100 μL, 10 mg $mL^{-1}$) were mixed with the ssDNA probe-MPs, followed by incubation at 20°C for 15 min. MNPs that have not bound to the MP were removed by five times of centrifugation. Lastly, the superstructures were resuspended in Tris-HCl (200 μL, 50 mM) for storage at 4°C.

**MicroRNA Detection Using DSN-Assisted Target Recycling.** For let-7b detection, 91.5 μL of the sample (containing target microRNA), 2.5 μL of RNase inhibitor (20 U $\mu L^{-1}$), 1 μL of DSN (1 U $\mu L^{-1}$) and 5 μL of core-satellite magnetic superstructures were mixed and incubated at 60°C for 1 h. After the reaction, separation was performed either by centrifugation (2000 g, 10 s) or standing (10 min) to separate the released MNPs from the MPs. Herein we chose centrifugation for the separation step. The suspension containing released MNPs was pipetted to a UV-transparent cuvette (REF 67.758.001, Nümbrecht, Germany) for optomagnetic measurement. Three independent measurements were performed for each sample.

**Optomagnetic Measurement.** The AC magnetic excitation field amplitude was 2.6 mT. The magnetic excitation field was applied perpendicular to the 405 nm laser beam. The light beam diameter and the optical path were 2 mm and 10 mm, respectively. During the optomagnetic measurement, 20 logarithmically equidistant points (30-3000 Hz) were recorded in 120 s.

**Scanning Electron Microscopy Characterization.** Three different core-satellite superstructures, *i.e.*, MP-RCA-NPs with high MNP load, MP-RCA-NPs with low MNP load and MP-NPs, were washed, resuspended in pure water and characterized by scanning electron microscopy (SEM, Zeiss-1530) to show the morphology and structure. An in-lens detector was utilized for detecting secondary electrons and the electron beam accelerating voltage was 5 kV.

**Endogenous MicroRNA Extraction.** Human cervical cancer cells (HeLa) were cultured in Dulbecco's Modified Eagle Medium (DMEM, Gibco) supplemented with 10% FBS and 100 IU $mL^{-1}$ penicillin streptomycin. The collected cells harvested by trypsinization were washed once with PBS (1×). The total RNA of the collected cells was extracted by the RNeasy mini kit (Qiagen, Hilden, Germany) and quantified by Nanodrop 1000 (Thermo Scientific). The qRT-PCR quantification of let-7b in the RNA extracts was performed by the Rudbeck Laboratory, Uppsala University.

## ASSOCIATED CONTENT

### Supporting Information

The Supporting Information is available free of charge on the ACS Publications website at DOI:

Calculation of the binding ratios between cores and satellites, standard curve for MNPs suspended in reaction buffer, concentrations of MNPs before and after DSN-assisted target recycling, sequences of oligonucleotides used in this study, and optomagnetic spectra for the stability study performed in FBS.

## AUTHOR INFORMATION

**Corresponding Author**

*E-mail:

mattias.stromberg@angstrom.uu.se

**Notes**

The authors declare no conflict of interest.

## ACKNOWLEDGMENTS

This research was financially supported by Swedish Research Council Formas (project numbers 221-2012-444 and 2011-1692).

## REFERENCES

(1) Kelley, S. O.; Mirkin, C. A.; Walt, D. R.; Ismagilov, R. F.; Toner, M.; Sargent, E. H. Advancing the speed, sensitivity and accuracy of biomolecular detection using multi-length-scale engineering. *Nat. Nanotechnol.* **2014,** *9*, 969-980.

(2) Huang, H. Y.; Lovell, J. F. Advanced Functional Nanomaterials for Theranostics. *Adv. Funct. Mater.* **2017,** *27*, 1603524.

(3) Syedmoradi, L.; Daneshpour, M.; Alvandipour, M.; Gomez, F. A.; Hajghassem, H.; Omidfar, K. Point of care testing: The impact of nanotechnology. *Biosens. Bioelectron.* **2017,** *87*, 373-387.

(4) Salem, A. K.; Searson, P. C.; Leong, K. W. Multifunctional nanorods for gene delivery. *Nat. Mater.* **2003,** *2*, 668-671.

(5) Cho, N. H.; Cheong, T. C.; Min, J. H.; Wu, J. H.; Lee, S. J.; Kim, D.; Yang, J. S.; Kim, S.; Kim, Y. K.; Seong, S. Y. A multifunctional core-shell nanoparticle for dendritic cell-based cancer immunotherapy. *Nat. Nanotechnol.* **2011,** *6*, 675-682.
(6) Cheng, Z. L.; Al Zaki, A.; Hui, J. Z.; Muzykantov, V. R.; Tsourkas, A. Multifunctional Nanoparticles: Cost Versus Benefit of Adding Targeting and Imaging Capabilities. *Science* **2012,** *338*, 903-910.
(7) Kostiainen, M. A.; Hiekkataipale, P.; Laiho, A.; Lemieux, V.; Seitsonen, J.; Ruokolainen, J.; Ceci, P. Electrostatic assembly of binary nanoparticle superlattices using protein cages. *Nat. Nanotechnol.* **2013,** *8*, 52-56.
(8) Mucic, R. C.; Storhoff, J. J.; Mirkin, C. A.; Letsinger, R. L. DNA-directed synthesis of binary nanoparticle network materials. *J. Am. Chem. Soc.* **1998,** *120*, 12674-12675.
(9) Nykypanchuk, D.; Maye, M. M.; van der Lelie, D.; Gang, O. DNA-guided crystallization of colloidal nanoparticles. *Nature* **2008,** *451*, 549-552.
(10) Zhang, Y. G.; Lu, F.; Yager, K. G.; van der Lelie, D.; Gang, O. A general strategy for the DNA-mediated self-assembly of functional nanoparticles into heterogeneous systems. *Nat. Nanotechnol.* **2013,** *8*, 865-872.
(11) Hong, F.; Zhang, F.; Liu, Y.; Yan, H. DNA Origami: Scaffolds for Creating Higher Order Structures. *Chem. Rev.* **2017,** *117*, 12584-12640.
(12) Sebba, D. S.; Mock, J. J.; Smith, D. R.; Labean, T. H.; Lazarides, A. A. Reconfigurable core-satellite nanoassemblies as molecularly-driven plasmonic switches. *Nano Lett.* **2008,** *8*, 1803-1808.
(13) Chou, L. Y.; Zagorovsky, K.; Chan, W. C. DNA assembly of nanoparticle superstructures for controlled biological delivery and elimination. *Nat. Nanotechnol.* **2014,** *9*, 148-155.
(14) Liong, M.; Im, H.; Majmudar, M. D.; Aguirre, A. D.; Sebas, M.; Lee, H.; Weissleder, R. Magnetic ligation method for quantitative detection of microRNAs. *Adv. Healthc. Mater.* **2014,** *3*, 1015-1019.
(15) Sun, M.; Xu, L.; Ma, W.; Wu, X.; Kuang, H.; Wang, L.; Xu, C. Hierarchical Plasmonic Nanorods and Upconversion Core-Satellite Nanoassemblies for Multimodal Imaging-Guided Combination Phototherapy. *Adv. Mater.* **2016,** *28*, 898-904.
(16) Zhao, X.; Xu, L.; Sun, M.; Ma, W.; Wu, X.; Kuang, H.; Wang, L.; Xu, C. Gold-Quantum Dot Core-Satellite Assemblies for Lighting Up MicroRNA In Vitro and In Vivo. *Small* **2016,** *12*, 4662-4668.
(17) He, L.; Brasino, M.; Mao, C.; Cho, S.; Park, W.; Goodwin, A. P.; Cha, J. N. DNA-Assembled Core-Satellite Upconverting-Metal-Organic Framework Nanoparticle Superstructures for Efficient Photodynamic Therapy. *Small* **2017,** *13*, 1700504.
(18) Wang, S. Z.; McGuirk, C. M.; Ross, M. B.; Wang, S. Y.; Chen, P. C.; Xing, H.; Liu, Y.; Mirkin, C. A. General and Direct Method for Preparing Oligonucleotide-Functionalized Metal-Organic Framework Nanoparticles. *J. Am. Chem. Soc.* **2017,** *139*, 9827-9830.
(19) Tian, B.; Ma, J.; Qiu, Z.; Zardán Gómez de la Torre, T.; Donolato, M.; Hansen, M. F.; Svedlindh, P.; Strömberg, M. Optomagnetic Detection of MicroRNA Based on Duplex-Specific Nuclease-Assisted Target Recycling and Multilayer Core-Satellite Magnetic Superstructures. *ACS Nano* **2017,** *11*, 1798-1806.
(20) Beyer, S.; Nickels, P.; Simmel, F. C. Periodic DNA nanotemplates synthesized by rolling circle amplification. *Nano Lett.* **2005,** *5*, 719-722.

(21) Deng, Z. X.; Tian, Y.; Lee, S. H.; Ribbe, A. E.; Mao, C. D. DNA-encoded self-assembly of gold nanoparticles into one-dimensional arrays. *Angew. Chem.* **2005**, *117*, 3648-3651; *Angew. Chem. Int. Ed.* **2005**, *44*, 3582-3585.
(22) Ali, M. M.; Li, F.; Zhang, Z.; Zhang, K.; Kang, D. K.; Ankrum, J. A.; Le, X. C.; Zhao, W. Rolling circle amplification: a versatile tool for chemical biology, materials science and medicine. *Chem. Soc. Rev.* **2014,** *43*, 3324-41.
(23) Russell, C.; Welch, K.; Jarvius, J.; Cai, Y. X.; Brucas, R.; Nikolajeff, F.; Svedlindh, P.; Nilsson, M. Gold Nanowire Based Electrical DNA Detection Using Rolling Circle Amplification. *ACS Nano* **2014,** *8*, 1147-1153.
(24) Zhao, W.; Gao, Y.; Kandadai, S. A.; Brook, M. A.; Li, Y. DNA polymerization on gold nanoparticles through rolling circle amplification: towards novel scaffolds for three-dimensional periodic nanoassemblies. *Angew. Chem. Int. Ed.* **2006**, *45*, 2409-2413.
(25) Yan, J.; Song, S.; Li, B.; Zhang, Q.; Huang, Q.; Zhang, H.; Fan, C. An on-nanoparticle rolling-circle amplification platform for ultrasensitive protein detection in biological fluids. *Small* **2010,** *6*, 2520-2525.
(26) Yan, J.; Su, S.; He, S.; He, Y.; Zhao, B.; Wang, D.; Zhang, H.; Huang, Q.; Song, S.; Fan, C. Nano rolling-circle amplification for enhanced SERS hot spots in protein microarray analysis. *Anal. Chem.* **2012,** *84*, 9139-9145.
(27) Yan, J.; Hu, C.; Wang, P.; Zhao, B.; Ouyang, X.; Zhou, J.; Liu, R.; He, D.; Fan, C.; Song, S. Growth and origami folding of DNA on nanoparticles for high-efficiency molecular transport in cellular imaging and drug delivery. *Angew. Chem. Int. Ed.* **2015**, *54*, 2431-2435.
(28) Zhu, Y.; Wang, H.; Wang, L.; Zhu, J.; Jiang, W. Cascade Signal Amplification Based on Copper Nanoparticle-Reported Rolling Circle Amplification for Ultrasensitive Electrochemical Detection of the Prostate Cancer Biomarker. *ACS Appl. Mater. Interfaces* **2016,** *8*, 2573-2581.
(29) Yin, B. C.; Liu, Y. Q.; Ye, B. C. One-step, multiplexed fluorescence detection of microRNAs based on duplex-specific nuclease signal amplification. *J. Am. Chem. Soc.* **2012,** *134*, 5064-5067.
(30) Degliangeli, F.; Kshirsagar, P.; Brunetti, V.; Pompa, P. P.; Fiammengo, R. Absolute and direct microRNA quantification using DNA-gold nanoparticle probes. *J. Am. Chem. Soc.* **2014,** *136*, 2264-2267.
(31) Lu, W.; Chen, Y.; Liu, Z.; Tang, W.; Feng, Q.; Sun, J.; Jiang, X. Quantitative Detection of MicroRNA in One Step via Next Generation Magnetic Relaxation Switch Sensing. *ACS Nano* **2016,** *10*, 6685-6692.
(32) Castaneda, A. D.; Brenes, N. J.; Kondajji, A.; Crooks, R. M. Detection of microRNA by Electrocatalytic Amplification: A General Approach for Single-Particle Biosensing. *J. Am. Chem. Soc.* **2017,** *139*, 7657-7664.
(33) Zhang, K.; Wang, K.; Zhu, X.; Xu, F.; Xie, M. Sensitive detection of microRNA in complex biological samples by using two stages DSN-assisted target recycling signal amplification method. *Biosens. Bioelectron.* **2017,** *87*, 358-364.
(34) Zhou, H.; Yang, C.; Chen, H.; Li, X.; Li, Y.; Fan, X. A simple G-quadruplex molecular beacon-based biosensor for highly selective detection of microRNA. *Biosens. Bioelectron.* **2017,** *87*, 552-557.
(35) Lu, J.; Getz, G.; Miska, E. A.; Alvarez-Saavedra, E.; Lamb, J.; Peck, D.; Sweet-Cordero, A.; Ebert, B. L.; Mak, R. H.; Ferrando, A. A.; Downing, J. R.; Jacks, T.; Horvitz, H. R.;

Golub, T. R. MicroRNA expression profiles classify human cancers. *Nature* **2005,** *435*, 834-838.
(36) Calin, G. A.; Croce, C. M. MicroRNA signatures in human cancers. *Nat. Rev. Cancer* **2006,** *6*, 857-866.
(37) Esquela-Kerscher, A.; Slack, F. J. Oncomirs - microRNAs with a role in cancer. *Nat. Rev. Cancer* **2006,** *6*, 259-269.
(38) Inui, M.; Martello, G.; Piccolo, S. MicroRNA control of signal transduction. *Nat. Rev. Mol. Cell Biol.* **2010,** *11*, 252-263.
(39) Lagos-Quintana, M.; Rauhut, R.; Lendeckel, W.; Tuschl, T. Identification of novel genes coding for small expressed RNAs. *Science* **2001,** *294*, 853-858.
(40) Valoczi, A.; Hornyik, C.; Varga, N.; Burgyan, J.; Kauppinen, S.; Havelda, Z. Sensitive and specific detection of microRNAs by northern blot analysis using LNA-modified oligonucleotide probes. *Nucleic Acids Res.* **2004**, *32*, e175.
(41) Thomson, J. M.; Parker, J.; Perou, C. M.; Hammond, S. M. A custom microarray platform for analysis of microRNA gene expression. *Nat. Methods* **2004,** *1*, 47-53.
(42) Li, W.; Ruan, K. MicroRNA detection by microarray. *Anal. Bioanal. Chem.* **2009,** *394*, 1117-1124.
(43) Chen, C.; Ridzon, D. A.; Broomer, A. J.; Zhou, Z.; Lee, D. H.; Nguyen, J. T.; Barbisin, M.; Xu, N. L.; Mahuvakar, V. R.; Andersen, M. R.; Lao, K. Q.; Livak, K. J.; Guegler, K. J. Real-time quantification of microRNAs by stem-loop RT-PCR. *Nucleic Acids Res.* **2005,** *33*, e179.
(44) Benes, V.; Castoldi, M. Expression profiling of microRNA using real-time quantitative PCR, how to use it and what is available. *Methods* **2010,** *50*, 244-249.
(45) Baker, M. MicroRNA profiling: separating signal from noise. *Nat. Methods* **2010,** *7*, 687-692.
(46) Shen, Y. T.; Tian, F.; Chen, Z. Z.; Li, R.; Ge, Q. Y.; Lu, Z. H. Amplification-based method for microRNA detection. *Biosens. Bioelectron.* **2015,** *71*, 322-331.
(47) Donolato, M.; Antunes, P.; Bejhed, R. S.; Zardán Gómez de la Torre, T.; Østerberg, F. W.; Strömberg, M.; Nilsson, M.; Strømme, M.; Svedlindh, P.; Hansen, M. F.; Vavassori, P. Novel Readout Method for Molecular Diagnostic Assays Based on Optical Measurements of Magnetic Nanobead Dynamics. *Anal. Chem.* **2015**, *87*, 1622-1629.
(48) Tian, B.; Bejhed, R. S.; Svedlindh, P.; Strömberg, M. Blu-ray optomagnetic measurement based competitive immunoassay for Salmonella detection. *Biosens. Bioelectron.* **2016,** *77*, 32-39.
(49) Mezger, A.; Fock, J.; Antunes, P.; Østerberg, F. W.; Boisen, A.; Nilsson, M.; Hansen, M. F.; Ahlford, A.; Donolato, M. Scalable DNA-Based Magnetic Nanoparticle Agglutination Assay for Bacterial Detection in Patient Samples. *ACS Nano* **2015,** *9*, 7374-7382.
(50) Tian, B.; Ma, J.; Zardán Gómez de la Torre, T.; Balint, A.; Donolato, M.; Hansen, M. F.; Svedlindh, P.; Strömberg, M. Rapid Newcastle Disease Virus Detection Based on Loop-Mediated Isothermal Amplification and Optomagnetic Readout. *ACS Sens.* **2016,** *1*, 1228-1234.
(51) Fock, J.; Jonasson, C.; Johansson, C.; Hansen, M. F. Characterization of fine particles using optomagnetic measurements. *Phys. Chem. Chem. Phys.* **2017,** *19*, 8802-8814.
(52) Williams, Z.; Ben-Dov, I. Z.; Elias, R.; Mihailovic, A.; Brown, M.; Rosenwaks, Z.; Tuschl, T. Comprehensive profiling of circulating microRNA via small RNA sequencing of cDNA

libraries reveals biomarker potential and limitations. *Proc. Natl. Acad. Sci. U. S. A.* **2013**, *110*, 4255-4260.

(53) Zhang, J.; Wu, D. Z.; Cai, S. X.; Chen, M.; Xia, Y. K.; Wu, F.; Chen, J. H. An immobilization-free electrochemical impedance biosensor based on duplex-specific nuclease assisted target recycling for amplified detection of microRNA. *Biosens. Bioelectron.* **2016,** *75*, 452-457.

(54) Deng, H. M.; Shen, W.; Ren, Y. Q.; Gao, Z. Q. A highly sensitive and selective homogenous assay for profiling microRNA expression. *Biosens. Bioelectron.* **2014,** *54*, 650-655.

(55) Pang, Y. F.; Wang, C. W.; Wang, J.; Sun, Z. W.; Xiao, R.; Wang, S. Q. Fe3O4@Ag magnetic nanoparticles for microRNA capture and duplex-specific nuclease signal amplification based SERS detection in cancer cells. *Biosens. Bioelectron.* **2016,** *79*, 574-580.

(56) Guo, L. H.; Lin, Y.; Chen, C.; Qiu, B.; Lin, Z. Y.; Chen, G. N. Direct visualization of sub-femtomolar circulating microRNAs in serum based on the duplex-specific nuclease-amplified oriented assembly of gold nanoparticle dimers. *Chem. Commun.* **2016,** *52*, 11347-11350.

(57) Zhang, K.; Wang, K.; Zhu, X.; Xie, M. H.; Zhang, X. L. A new method for sensitive detection of microphthalmia-associated transcription factor based on "OFF-state" and "ON-state" equilibrium of a well-designed probe and duplex-specific nuclease signal amplification. *Biosens. Bioelectron.* **2017,** *87*, 299-304.

(58) Donolato, M.; Antunes, P.; Zardán Gómez de la Torre, T.; Hwu, E. T.; Chen, C. H.; Burger, R.; Rizzi, G.; Bosco, F. G.; Strømme, M.; Boisen, A.; Hansen, M. F. Quantification of rolling circle amplified DNA using magnetic nanobeads and a Blu-ray optical pick-up unit. *Biosens. Bioelectron.* **2015,** *67*, 649-655.

(59) Weber, J. A.; Baxter, D. H.; Zhang, S. L.; Huang, D. Y.; Huang, K. H.; Lee, M. J.; Galas, D. J.; Wang, K. The MicroRNA Spectrum in 12 Body Fluids. *Clin. Chem.* **2010,** *56*, 1733-1741.

(60) Tian, B.; Wetterskog, E.; Qiu, T.; Zardán Gómez de la Torre, T.; Donolato, M.; Hansen, M. F.; Svedlindh, P.; Strömberg, M. Shape anisotropy enhanced optomagnetic measurement for prostate-specific antigen detection via magnetic chain formation. *Biosens. Bioelectron.* **2017,** *98*, 285-291.

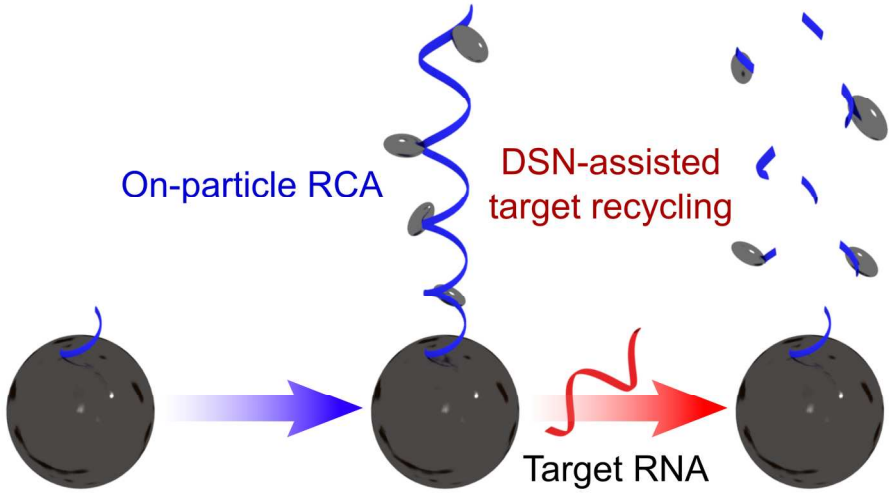


TOC